ICEM12- 12th International Conference on Experimental Mechanics
29 August - 2 September, 2004 Politecnico di Bari, Italy

# Structured light projection for accurate 3D shape determination

Ø. Skotheim, F. Couweleers

*SINTEF ICT, Dept. of Photonics, 7465 Trondheim, NORWAY, oystein.skotheim@sintef.no*

## ABSTRACT

Structured light projection systems can be used in a wide range of applications where information about shape or shape deviations is required, from macro- to nano-scale. Systems we have developed, based on projected structured light, combining Gray code and phase shifting fringe projection and using off-the shelf components like B/W CCD cameras and multi-media data projectors, provide robust height measurement images with a high resolution at a low cost. By carefully observing a number of parameters, it is possible to attain this high resolution in a large measurement volume even with low-cost, off-the-shelf components. We are able to achieve a noise floor in phase determination of 30 mrad, which translates to a measurement resolution of 1 part in 10,000 of the object size. The ability to project high contrast structured light patterns in different scales allows the use of this method with this relative resolution from overall shape determination to surface roughness measurements. When we have accurate 3D profiles, subsequent processing and extraction of mechanical parameters such as roughness parameters, wear, faults, sizes, angles and radii is possible. This extraction can be customised to each new application.

## 1. INTRODUCTION

Structured light has reached a high popularity in recent years as a method for 3D shape measurement. Some of its advantages are that it is fast, contactless, working in full-field and that a measurement system can be made very cheap by using off-the-shelf components.

## 2. STRUCTURED LIGHT

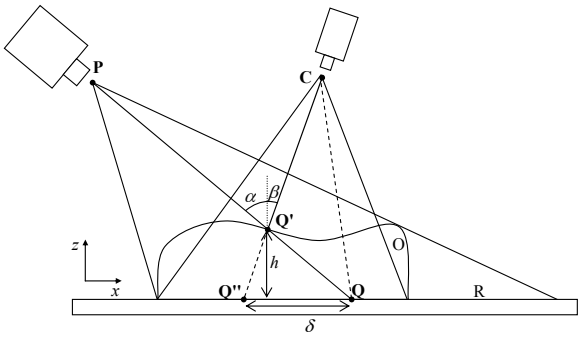


**Figure 1:** Geometry of structured light setup

The geometry of our setup for structured light is shown in figure 1. **P** denotes the exit pupil of the projector while **C** denotes the entrance pupil of the camera. R denotes a plane reference surface which defines the zero-level height. The projector illuminates the scene with a pattern of light stripes parallel to the y-axis and perpendicular to the plane of the paper. One ray from the projector is drawn from **P** to a point **Q** on the reference plance. When the object O is introduced, the ray from the projector intercepts the surface at the point **Q'** on the object. This

is visible in the camera as a displacement, $\delta$ = |**Q''Q**|. It is easy to show that the relation between the displacement, $\delta$ and the height, *h,* in this point is given by

$$h = \frac{\delta}{\tan\alpha + \tan\beta} \tag{1}$$

Because the projector and camera are at finite distances, the angles $\alpha$ and $\beta$ vary significantly over the field of view. The equation in (1) is therefore rarely used in practice. Different approaches for determining height from a measure of the stripe displacement is discussed in section 3.1.

### 2.1 Phase stepping

The scene is illuminated with a series of shifted cosine patterns. The intensity distribution in such a pattern can be represented as

$$I_n(x,y) = I_0(x,y)\left[1 + R(x,y)\cos(2\pi \tfrac{N}{W} x + n\tfrac{\pi}{4})\right] \quad n \in \{0,1,2,3\} \tag{2}$$

where $I_0(x,y)$ corresponds to the background illumination, *R(x,y)* is the object reflectance in each point, *N* is the number of fringes and *W* is the width of the image in pixels. A four step phase-stepping algorithm was chosen with $\pi/2$ steps as a compromise between measurement time and sensitivity to noise. The four equations can be easily solved to yield the phase [3]:

$$\phi(x,y) = \arctan\left(\frac{I_4(x,y) - I_2(x,y)}{I_1(x,y) - I_3(x,y)}\right) \tag{3}$$

The phase of a cosine function is a linear function, and hence can be used as a direct measure for the displacement of the pattern ($\delta$). Because the equation involves only a ratio between intensities, the background, $I_0$ and the surface reflectance, *R(x,y)* is effectively canceled out.

The phase, $\phi(x,y)$ is obtained in the interval $[0,2\pi]$ and is therefore only piecewise continuous. It needs to be unwrapped to obtain a true profile. Phase unwrapping is a trivial operation only for smooth objects given a high signal-to-noise ratio and it can give rise to unpredictable errors if this is not the case. Worse, the size of steep features on the object surface cannot be determined unless it gives rise to a phase change, $\Delta\phi < 2\pi$.

### 2.2 Gray code patterns

To eliminate the need of phase unwrapping, we need to be able to distinguish individual light stripes from each other in the field of view. One approach which is commonly described in literature [2] is to introduce a time-encoded binary code with each position in the pattern. The code can be generated by illuminating the scene with a series of binary patterns and threshold the sequence of transitions that occur between dark and bright at each location. An example is shown in figure 2, where we have chosen two distinct locations in a planar scene and followed the transitions that occur here as we project a sequence of 6 binary patterns onto it.

**Figure 2**: Gray code patterns (n=6)

The upper arrow indicates the transitions that occur at position A, whilst the lower arrow indicates the transitions at position B. If we denote darkness with 0 and brightness with 1, we can describe the transitions that occur at position A as the binary word 001100. Likewise, the binary word for position B becomes 101110. Because our code consists of 6 binary digits, we are able to distinguish $2^6$=64 separate locations in the pattern.

The coding scheme that we have used is called Gray code, and is composed in such a way that successive numbers differ by at most one digit in their binary words. This coding scheme ensures that the error is minimized if one of the transitions is erroneously detected. We have chosen to extend the code with two additional patterns, one where the projector is switched to black and one where it is switched to white. This allows variations in the object's reflectivity and in the environmental light levels without adding too much to the measurement time [2].

### 2.3 Combination of Gray Code and phase stepping

It should be clear from section 2.1 that phase stepping yields piecewise continuous height profiles with high accuracy, but breaks down if the object has steep features. On the other hand, illumination with a sequence of Gray code patterns yields absolute height values but only with very poor resolution.

As suggested by [2], the techniques can be combined. By choosing a number of sinusoidal fringes which is equal to $2^n$, the fringes can be aligned with the binary transitions in a sequence of $n$ Gray code patterns. The resulting Gray code words, GC(x,y) and the values obtained for the phase, $\varphi(x,y)$, can be simply added together to form a continuous function which describes the absolute fringe position in each position in the field of view:

$$GCPS(x,y) = \mathrm{GC}(x,y) + \tfrac{1}{2\pi}\varphi(x,y) \tag{4}$$

## 3. CALIBRATION

### 3.1 Height calibration

As can be seen from equation 1, the height depends on the angles $\alpha$ and $\beta$. These angles vary significantly over the image unless the projector and the camera reside in infinity. Assuming that $\alpha$ and $\beta$ depend only on $x$ and $y$, we can introduce a calibration factor, $C(x,y)$, which relates the measured GCPS values to height in metric units. $C(x,y)$ can be calculated by performing a a measurement on a surface at two known heights, $z=h_1$ and $z=0$:

$$\begin{aligned} h_1 &= C(x,y)\cdot\left[GCPS(x,y,h_1) - GCPS(x,y,0)\right] \\ C(x,y) &= \frac{h_1}{\left[GCPS(x,y,h_1) - GCPS(x,y,0)\right]} \end{aligned} \tag{5}$$

While this calibration is very simple to perform, the results are not very good. In reality the calibration factor depends also on $z$. This implies that $C(x,y)$ has a functional dependence on $\Delta GCPS(x,y) = GCPS(x,y,h)-GCPS(x,y,0)$. Assuming as a first approximation that this dependence is linear, $C(x,y)=C_1(x,y)\cdot\Delta GCPS(x,y)+ C_2(x,y)$, the relationship between $h(x,y)$ and $\Delta GCPS(x,y)$ can be written as

$$h(x,y) = a(x,y)\cdot\Delta GCPS(x,y)^2 + b(x,y)\cdot\Delta GCPS(x,y) \tag{6}$$

The calibration factors *a(x,y)* and *b(x,y)* can be calculated by measuring a surface at three distinct known height levels, namely $z=h_1$, $z=h_2$ and $z=0$. Solving the system for the two unknowns yields:

$$b(x,y) = \frac{h_2 \cdot \Delta GCPS(x,y,h_1) - h_1 \cdot \Delta GCPS(x,y,h_2)^2}{\Delta GCPS(x,y,h_1)^2 \cdot \Delta GCPS(x,y,h_2) - \Delta GCPS(x,y,h_1) \cdot \Delta GCPS(x,y,h_2)^2}$$
$$a(x,y) = \frac{h_1 - b(x,y) \cdot \Delta GCPS(x,y,h_1)}{\Delta GCPS(x,y,h_1)^2} \quad (7)$$

We have seen from practical experience that a fourth order polynomial in *x* and *y* represents well the basic shape of the measured surface, while eliminating the undesired high-frequency noise components. This means that we can measure only a few points at each height level, *h*, from which we can interpolate the *ΔGCPS(x,y,h)* functions by fitting these points to a polynomial surface. Instead of translating a reference plane to different height levels, we have chosen to distribute one or more small calibration objects with accurately known height in the camera's field of view and perform one or more GCPS measurements.

Table 1 shows the results of some height measurements performed on a stairway shaped object. The values in the leftmost column shows the height values as measured with calipers, while the central and right columns show the values obtained from structured light using first order and second order height calibration respectively. The values used for the calibration heights were $h_1$=49.79mm and $h_2$=99.58mm. The uncertainties in the height determinations were about ±0.2mm for the mechanical as well as for the optical measurements.

**Table 1:** Mechanically and optically measured heights on a stairway shaped object

| True height | Measured height (1st order calibration) | Measured height (2nd order calibration) |
|---|---|---|
| 5.1 | 4.1 | 4.8 |
| 15.1 | 12.8 | 14.6 |
| 20.1 | 17.3 | 19.6 |
| 25.2 | 21.9 | 24.7 |
| 30.2 | 26.5 | 29.7 |
| 35.2 | 31.2 | 34.7 |

The height levels $h_1$ and $h_2$ should be chosen according to the expected object size. For example, for an expected object size of less than 100mm, choosing $h_1$=50.0mm and $h_2$=100.0mm would be a good choice. Note that the calibration heights used in the example above were not optimal.

### 3.2 Intensity calibration

The equations for phase-stepping assume that we are able to project patterns with pure sinusoidal intensity variations across the fringes. In practice, a discrete version of equation 2 is used to generate a digitized pattern which resembles a sine pattern as closely as possible. The dashed line in figure 3 shows the measured intensity as patterns with uniform intensity values gradually rising from 0 to 255 are projected onto a plane, white surface. It has been shown earlier that a non-quadratic non-linearity in the transfer gives rise to an error component with high spatial frequency in the phase determination of the four-step algorithm [1,4]. By creating an inverse look-up table from the data in figure 3, we can compensate for the projector's non-linear behavior, and hence reduce the error made in the phase-stepping algorithm. Refer to [1] for a more detailed error analysis.

Previously reported efforts, e.g. [6], does not take into account the cross talk between pixels that occur, especially in LCD projectors, when sine patterns of high frequency are projected in stead of uniform intensity patterns. The solid line in figure 3 shows the measured intensity as a pattern of 64 sinusoidal fringes with gradually increasing initial phase are projected onto the surface. It is evident that the contribution from cross-talk is significant. For this reason, we have chosen to use a series of sinusoidal fringes to generate an inverse look-up table to ensure that the projected patterns resemble closely a true sinusoid.

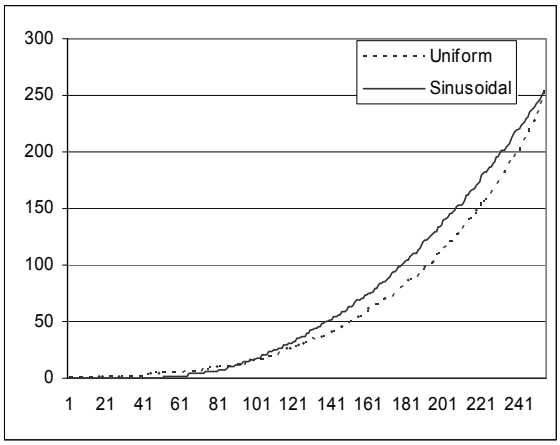


**Figure 3**: Measured intensity when a series of patterns with gradually rising uniform intensity (dashed line) and sinusoidal intensity (solid line) are projected onto a plane, white surface.

Figure 4 shows a section of a GCPS measurement performed on a planar surface elevated 5mm above the reference plane. (The GCPS values are mapped to grayscale values with increasing intensity) The image to the right illustrates the high-frequency periodic noise which appears due to the non-linear response of the projector. The image to the left has been corrected via an inverse look-up table which also takes into account cross-talk between pixels. It is evident that the systematic noise has been eliminated, and what is left is noise of more random character (which is believed to be mostly due to photon shot noise [1]). Figure 5 illustrates the same phenomenon, but this time as a cross section vertically across the fringes before and after non-linear intensity compensation. The RMS value of the random noise is approximately $4 \cdot 10^{-3}$. In the case of 64 fringes, this corresponds to approximately 1/16.000 of the camera's field of view.

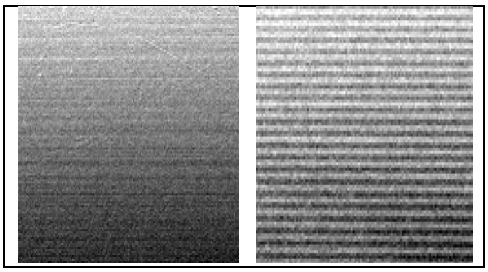

**Figure 4:** Section of measurement on 5mm high planar object with (left) and without (right) intensity calibration.

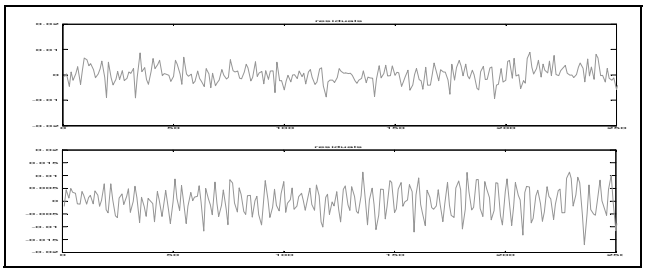

**Figure 5:** GCPS values measured across fringes with intensity calibration (upper graph) and without intensity calibration (lower graph).

### 3.3 XY calibration

The equations given in 5-7 allow accurate height values to be calculated for each pixel in the camera image. However, to be able to measure true 3D coordinates, we need to establish a relationship between a point on the three-dimensional object, *(x,y,z),* and a pixel position, $(b_x,b_y)$, in the camera image:

We have chosen to use standard camera calibration theory (primarily used for photogrammetry and stereo vision) to calibrate our structured light system [5,7,8].

The model assumes three steps:

1. Rigid-body transformation (rotation + translation) from object coordinates, *(x,y,z)*, to coordinates centered in the camera's principal point, *(x',y',z')*
2. Perspective projection (through pinhole)
3. Distortion (radial and tangential)

The parameters used in step 1 of the model are called extrinsic parameters, while the parameters used in step 2 and 3 are called the intrinsics parameters. There are a total of about 20 parameters in this model. To solve the equations for the unknowns, a chessboard pattern is placed in several different poses in the camera field of view. A corner detection algorithm is applied to detect the sub-pixel position of the inner corners of the chessboard pattern. The detected points are fitted to the model and the parameters are estimated. After the intrinsics parameters have been estimated, an image is recorded with the chessboard pattern placed on the reference surface which spans the zero-level height plane. This allows the absolute location and orientation of the reference plane to be determined. The excellent MATLAB Camera Calibration Toolbox by Jean-Yves Bouguet [8] is being used for the entire process described above.

When the extrinsics and intrinsics parameters are found, the process can be reversed to find the object coordinates, *(x,y,z)*, that correspond to each pixel $(b_x, b_y)$. The distortion is first removed numerically from the camera image by an iterative approach [5]. The equations from step 1 and 2 are then combined and solved to yield the desired object coordinates *(x,y,z)* where $z = h(x,y)$ is determined from structured light.

## 4. EXAMPLES OF APPLICATIONS

### 4.1 Industrial inspection of car parts

An inspection system has been developed to replace manual inspection in a Norwegian production line for car parts [1]. The system is designed to measure the shape of a particular part, detect possible faults that are present as more or less localized deviations of the part's shape compared to a model, and sort the parts according to the subsequent pass/ fail decision. Standard, off-the-shelf components have been used: SVGA resolution liquid crystal data projectors and B&W video cameras. The system is able to find geometrical faults as small as 2x2x0.25mm in a part that measures roughly 400x400x15mm [1]. The use of 4 cameras, 3 projectors and a turning operation allows measurements to be performed on all sides of the complex shape part within a time slot of approximately 10 seconds. Figure 6 shows a top view of the car part illuminated with one of the patterns in the Gray code sequence along with the obtained 3D model. The rightmost image shows a close-up of two small cracks at the side of the part. The gray scales represent height in millimeters.

The error detection was based on comparing the part with a model. The model was designed by using height measurements of a number of normal parts. Figure 7 shows a measured part together with the model and a difference image. The difference image shows an example of a process-related shape deviation.

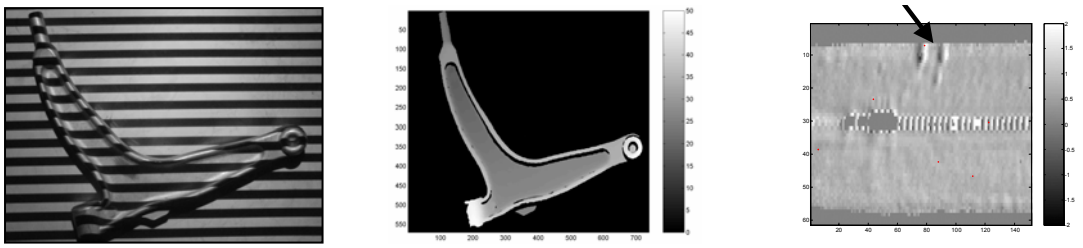

**Figure 6:** Car part illuminated by structured light (left), obtained 3D model (center) and close-up of two small cracks at the side of the part (right)

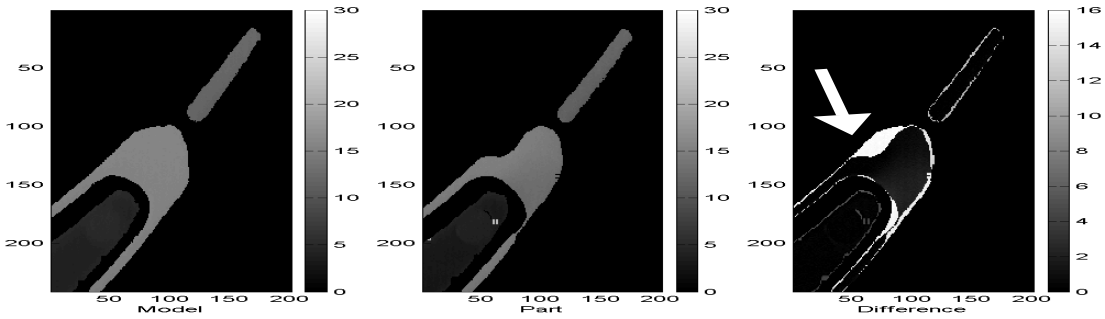


**Figure 7:** Image of model and part together with the difference image.

## 4.2 Markerless registration for minimally-invasive surgery

In an ongoing project, our group is working on an instrument for use in non-invasive surgery. The purpose is to combine in-situ measurements of the anatomy of the patients with preoperative data (e.g. tomography or magnetic resonance images). The preoperative data is segmented to make surface models of the organs that are influenced by the operation. By matching this data with surface measurements performed with structured light, we are able to determine the accurate absolute position of the organs in the globally defined coordinate system of the surgery room.

Figure 8 displays some measurements performed on the face of the authors with our structured light shape measurement system. The results obtained are point clouds of calibrated (x,y,z) triples in a globally defined coordinate system. The absolute accuracy of each point in the point cloud is approximately ±0.5mm.

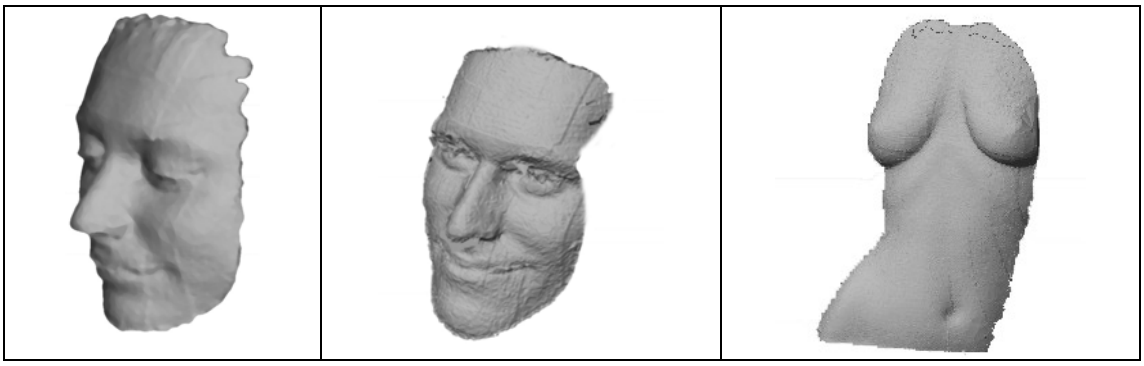

**Figure 8:** 3D surfaces of the face of the authors (left and centre) and torso (right) obtained from our shape measurement system based on structured light.

## 5. CONCLUSION

We have discussed the basis for our shape measurement system based on a combination of Gray code illumination and phase-stepping fringe projection. Measuring the phase in the fringe pattern rather than intensity levels in images yields a high independence of variations in surface characteristics. Use of the Gray code illumination makes phase unwrapping of phase maps obsolete, which in turn allows steep or isolated object features to be measured. To reduce the costs of the hardware as much as possible, we have used standard B&W video cameras and SVGA resolution LCD video projectors. The study of geometric models of structured light systems has shown that a second order calibration routine yields highly accurate results for object height with respect to a reference plane. Curve fitting in 3 dimensions allows reduction of noise and the use of simple, low cost calibration tools. Camera calibration routines otherwise known from photogrammetry and stereo vision allow reduction of errors and accurate determination of lateral coordinates. A special projector calibration routine which takes into account the cross talk between pixels has allowed us to reach a noise floor in our height measurements of less than 1 part in 10.000 of the field of view. Examples have been shown for industrial inspection of car parts and for registration of the patient's anatomy in non-invasive surgery. Ongoing research is focusing on stitching of data from several viewing angles, reduction of data by fitting the measured point clouds to spline surfaces and interaction with CAD software for reverse engineering applications.

## BIBLIOGRAPHY


[1] F. Couweleers, Ø. Skotheim, H. Schulerud, K. Kaspersen, "In-line geometric fault detection in car parts based on structured light projection and image processing", Proc. SPIE Vol. 5144 (2003)

[2] Giovanna Sansoni, Matteo Carocci and Roberto Rodella, “Three-dimensional vision based on a combination of gray-code and phase-shift light projection: analysis and compensation of the systematic errors”, Applied Optics, 38, 6565-6573, 1999.

[3] Y. Y. Hung et al, "Practical three-dimensional computer vision techniques for full-field surface measurement", Optical Engineering. 39 (1) 143-149, 2000.

[4] R. Zumbrunn, "Automated Fast Shape Determination of Diffuse Reflecting Objects at Close Range, by Means of Structured Light and Digital Phase Measurement", *ISPRS Intercommission Conference on 'Fast Processing of Photogrametric Data'*, 363-379, Interlaken, 1987

[5] J. Heikkilä and O. Silvén, "A Four-step Camera Calibration Procedure with Implicit Image Correction", Proceedings of IEEE Computer Vision and Pattern Recognition, Puerto Rico, 1997

[6] Peisen S. Huang, Qingying J. Hu, and Fu-Pen Chiang, “Double three-step phase-shifting algorithm*”, Applied Optics*, **41**, 4503-4509, 2002

[7] Jean-Yves Bouguet: Visual methods for three-dimensional modeling. PhD Thesis, California Institute of Technology [http://www.vision.caltech.edu/bouguetj/thesis/thesis.html]

[8] Camera Calibration Toolbox for Matlab [http://www.vision.caltech.edu/bouguetj/calib_doc/index.html]